Image Cover Sheet

CLASSIFICATION	SYSTEM NUMBER 516581
UNCLASSIFIED	

TITLE

Carrier detection of PSK signals

System Number: 516581

Patron Number:

Requester:

Notes:

DSIS Use Only:

Deliver to:

This page is left blank

This page is left blank

Carrier Detection of PSK Signals

Douglas A. Hill and John B. Bodie

***Abstract*—This paper reports on a theoretical study of the detection of the $2f$ and $4f$ carrier components of phase-shift keying (PSK) signals produced by passing signal and noise through a nonlinear device. Unbalanced quadrature PSK (QPSK) signals, i.e., QPSK signals with unequal power in the two channels, are studied. The complete range of channel power ratio is covered, with equal emphasis on the general unbalanced case and the two limiting cases of binary PSK and (balanced) QPSK. Analytic expressions are derived for the detected SNR of carrier harmonics $2f$ and $4f$ as a function of SNR, channel power ratio, and normalized input bandwidth. The results apply equally well to PSK data signals and direct-sequence spread-spectrum signals. Measurements confirm every aspect of the theory. The least detectable signal type is balanced QPSK, which is detectable (at $4f$) at a threshold SNR ranging from -2 to -13 dB as the detection process gain (chip or data rate/detection bandwidth) is varied from 40 to 80 dB.**

***Index Terms*—Carrier detection, phase-shift keying, pseudo-noise code communication, quadrature phase-shift keying, signal detection.**

I. Introduction

WHEN A phase-shift keying (PSK) signal with noise is passed through a nonlinear device, detectable components of multiples of the carrier frequency (f) are created. Detection of these carrier components may be used either as the first step in carrier recovery for coherent demodulation of a signal, or as a means of detection of covert direct-sequence spread-spectrum (DSSS) signals. We analyze the latter case here, but the results apply to the former case as well—hence, the more generic title.

A survey of the unclassified peer-reviewed literature on carrier detection of PSK signals is found in the previous paper [1]. Gardner and Spooner [2] also present a useful comparison and discussion of the detection performance of the radiometer, chip-rate detector and $2f$ carrier detector used with binary PSK (BPSK), quadrature PSK (QPSK), SQPSK, and minimum-shift keying signals. Briefly, the situation is as follows: detection of the $2f$ carrier component of BPSK signals has been fairly well analyzed (as reviewed in [1]). There has been one published quantitative analysis of the detection of the $4f$ carrier component of QPSK signals [1]. Both chip-rate and carrier detectors perform better than the radiometer in terms of discriminating against interfering signal power or varying noise levels [2], and both also accurately determine one characteristic signal frequency (the first step in signal identification and exploitation). The only published measurements for BPSK carrier detection at $2f$ and QPSK carrier detection at $4f$ are in [1] and [3]. With the exception of our own recently published companion paper [4], carrier detection of unbalanced quadrature phase-shift-keyed (UQPSK) signals, i.e., QPSK signals with unequal power in the two channels, has never been studied, either theoretically or experimentally.

This paper reports on a theoretical study of the detection of unbalanced QPSK (UQPSK) signals above and below an additive white Gaussian noise (AWGN) floor using nonlinear methods to generate the $2f$ and $4f$ carrier components. For UQPSK signals, the channel power ratio p is defined as (Q-channel power)/(I-channel power). The complete range of channel power ratio ($0 \leq p \leq 1$) is studied, with equal emphasis on the general unbalanced case and the two limiting cases of BPSK ($p = 0$) and balanced QPSK ($p = 1$). (UQPSK is occasionally used for satellite digital communications, typically with a channel power ratio of 0 to -5 dB [5].) Measurements confirming the theory are presented in [1] for BPSK and QPSK modulations, and here for UQPSK modulation with arbitrary p.

Although derived with the DSSS case in mind, the results apply equally to carrier detection of any PSK signal at arbitrary SNR—with the data rate replacing the chip rate in the theory. For DSSS signals below noise, the motivation is to find the channel power ratio which minimizes the detectability of either carrier harmonic. For PSK data signals above noise, the motivation is to determine which carrier component is most easily recovered at each channel power ratio. Since practical carrier recovery is desirable in both applications, carrier harmonics must be continuously recoverable, not merely detectable. This requirement precludes the use of cyclostationary detection techniques.

II. Theory

For generality, we label the two quadrature channels as A and B without labeling one "in-phase" and the other "quadrature." We define the unbalanced QPSK signal of interest at the input to the nonlinearity as

$$s(t) = \sqrt{P_a}[c_a(t)d_a(t)\cos(2\pi ft) + \sqrt{p}c_b(t)d_b(t)\sin(2\pi ft)] \quad (1)$$

where P_a is the baseband power in the A channel, f is the carrier frequency, and p is the channel power ratio ($0 \leq p \leq 1$). $c_a(t)$ and $c_b(t)$ are the A and B channel baseband chip sequences, and $d_a(t)$ and $d_b(t)$ are the A and B channel baseband data sequences, respectively. Equation (1) includes the two limiting

Paper approved by B. L. Hughes, the Editor for Theory and Systems of the IEEE Communications Society. Manuscript received May 26, 1999. This work was supported by the Canadian Department of National Defence.

D. A. Hill is with the Defence Research Establishment Ottawa, Department of National Defence, Ottawa, ON K1A 0Z4, Canada (e-mail: douglas.hull@dreo.dnd.ca).

J. B. Bodie was with Calian Communications Systems Ltd., Kanata, ON< Canada. He is now with Square Peg Communications Inc., Ottawa, ON K2K 2A3, Canada (e-mail: bodie@squarepeg.ca).

Publisher Item Identifier S 0090-6778(01)02177-8

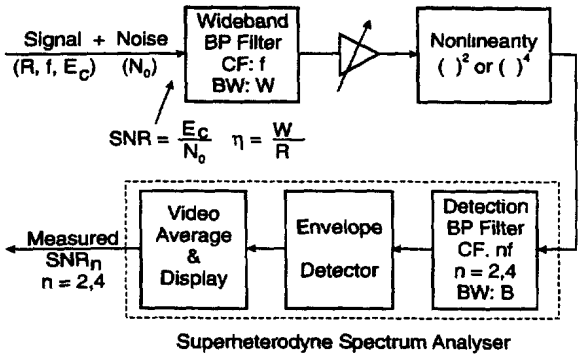

Fig. 1 Carrier detection system.

cases of BPSK ($p = 0$ or $-\infty$ dB) and QPSK ($p = 1$ or 0 dB). The chip rate R is not shown explicitly in (1).

As illustrated in Fig. 1, the carrier detection system consists of a nonlinear device preceded by a wide-band band-pass filter and followed by a superheterodyne spectrum analyzer which provides narrow-band filtering and envelope detection of the chosen carrier component. The signal, together with AWGN of one-sided power spectral density (PSD) N_0, is passed through the wide-band band-pass filter of noise-equivalent bandwidth W, centered at f. Results are expressed in terms of the normalized bandwidth, $\eta = W/R$ ($0.2 \le \eta \le 8$). The signal-to-noise ratio (SNR) at the input to the wide-band filter is defined as $\mathrm{SNR} \equiv (\text{prefilter signal power})/N_0R = E_C/N_0$, where E_C is the chip symbol energy of the prefilter signal. After passing through the wide-band filter and ideal nonlinearity (described below), the resulting combination of signal and noise is passed through a narrow-band detection filter (in the spectrum analyzer) of bandwidth $B \ll W$ centered at the detection frequency of $2f$ or $4f$ and finally detected with the spectrum analyzer's envelope detector. The averaged SNR of the carrier components at the output of the detection system is denoted SNR_n with $n = 2$ or 4.

The theories for SNR_2 and SNR_4 for UQPSK signals with arbitrary p and η are developed in Appendix A. The calculations assume that the nonlinearity is a perfect squaring operation for generation of $2f$ components, and a perfect quadrupling operation for generation of $4f$ components. The signal's unfiltered chips and data bits are taken to be statistically independent zero-mean random variables with equiprobable values of ± 1. The transmitted signal is considered to be only weakly band-pass filtered, but this is an acceptable simplification of the problem because the most useful results will be shown to be near $\eta = 1$, where the receive filter bandwidth dominates. Only a fraction $F(\eta)$ ($0 \le F(\eta) \le 1$) of the initial signal power passes through the wide-band band-pass filter. Our definition of $F(\eta)$ neglects passband attenuation, which affects signal and noise equally. For simplicity, $F(\eta)$ is calculated (in (A3) of Appendix A) for a brick-wall filter centered on a sinc^2 spectrum.

The theoretical SNR_2 for UQPSK signals with arbitrary p and η is (from (A7) in Appendix A)

$$\mathrm{SNR}_2 = \frac{(\eta R/B)(1-p)^2 F^2\,\mathrm{SNR}^2}{2\eta^2(1+p)^2 + 4\eta(1+p)^2 F\,\mathrm{SNR} + S_2F^2\,\mathrm{SNR}^2} \quad (2)$$

TABLE I
KEY PARAMETERS AS A FUNCTION OF NORMALIZED INPUT BANDWIDTH η

η	$F(\eta)$	β_{22}*	β_4*	p_{null} (dB)	
				Calc.§	Meas.
0	0	1	3	0	—
0.50	0.467	1.00	1.93	- 4.38	- 3.9
1.00	0.773	1.018	1.325	- 6.42	- 6.5
2.00	0.902	1.07	1.15	- 7.32	- 7.3
∞	1	1	1	- 7.66	- 7.6

* Calculated for a 3rd order Butterworth bandpass filter. § Calculated from (6).

where $S_2 \equiv [(1+p^2)(\beta_4-1)+2p(\beta_{22}+1)]$ and the dependence on η is both explicit in (2) and implicit in $F = F(\eta), \beta_4(\eta)$ and $\beta_{22}(\eta)$. β_4 and β_{22} are two of the signal distortion coefficients $\{\beta_i\}$ and $\{\beta_{ij}\}$ which describe the distortions in baseband waveforms caused by band-pass filtering. These are defined in (A5) of Appendix A and calculated in Appendix B. Representative values of $F(\eta), \beta_4(\eta)$ and $\beta_{22}(\eta)$ are presented in Table I. For QPSK signals ($p = 1$), (2) gives $\mathrm{SNR}_2 = 0$, confirming that there is no power at $2f$ from a squared (balanced) QPSK signal.

SNR_2 for BPSK signals is, (from (2) with $p = 0$)

$$\mathrm{SNR}_2 = \frac{(\eta R/B)F^2\,\mathrm{SNR}^2}{2\eta^2 + 4\eta F\,\mathrm{SNR} + [\beta_4 - 1]F^2\,\mathrm{SNR}^2}. \quad (3)$$

The mid-to-low SNR limit of (3), which neglects the SNR^2 term in the denominator, is

$$\mathrm{SNR}_2 = \frac{(R/2B)F^2\,\mathrm{SNR}^2}{\eta + 2F\,\mathrm{SNR}}. \quad (4)$$

This formula, with suitable changes in the definition of input SNR, was previously derived for any weakly-filtered constant-envelope double-sideband signal [6, eq. (11)] and also more specifically derived for BPSK signals with arbitrary η [7, eq. (30)]. It is also inherent in the equations derived using the cyclostationary analysis [2, eq. (42)]. For the most useful range of applications ($\eta \ge 1$ and $\mathrm{SNR} \le 0$ dB), the maximum error in SNR_2 using this approximation is 0.2 dB (which occurs at $\eta = 1$ and $\mathrm{SNR} = 0$ dB). For BPSK signals at very low SNR, $\mathrm{SNR}_2 \propto \mathrm{SNR}^2$.

The theoretical SNR_4 for UQPSK signals with arbitrary p and η is, from (A11)

$$\begin{aligned}\mathrm{SNR}_4 &= (3\eta R/2B)\gamma_4 F^4\,\mathrm{SNR}^4/\mathrm{Denom}\\ \mathrm{Denom} &= 24(1+p)^4\eta^4 + 96(1+p)^4\eta^3 F\,\mathrm{SNR}\\ &\quad + 72(1+p)^2 Q_2\eta^2 F^2\,\mathrm{SNR}^2\\ &\quad + 16(1+p)Q_1\eta F^3\,\mathrm{SNR}^3 + S_4F^4\,\mathrm{SNR}^4 \quad (5)\end{aligned}$$

where Q_1, Q_2, S_4, and $\gamma_4 \equiv [\beta_4(1+p^2) - 6p\beta_{22}]^2$ [defined by (A9) and (A10)] are functions of $p, \{\beta_i\}$, and $\{\beta_{ij}\}$.

A null in SNR_4 is predicted by (5) whenever p is set to make γ_4 zero. That value is

$$p_{\text{null}} = \left(3\beta_{22} - \sqrt{9\beta_{22}^2 - \beta_4^2}\right) \Big/ \beta_4. \quad (6)$$

The null is explained as follows. The UQPSK signal has four phase states, which are spaced 90° apart only for balanced QPSK. The quadrupled UQPSK signal also has four phase states in general, but for a particular critical value of $p = p_{\text{null}}$, the quadrupled carrier spends equal time in just two opposing phase states (i.e., 180° apart). This new signal is similar to a BPSK signal of carrier frequency $4f$, and thus has a "suppressed carrier," with no average power, at $4f$. For unfiltered UQPSK, $\beta_{22} = \beta_4 = 1$ and (6) gives $p_{\text{null}} = 3 - \sqrt{8} = 0.1716$ or -7.66 dB. This corresponds to a phase angle of $\pi/8$. That is, in the carrier phase signal constellation, $p_{\text{null}} = \tan^2(\pi/8)$ and the four phase states are $(\pm\pi/8, \pi \pm \pi/8)$. When these phases are quadrupled, the new states coincide at the two states, $\pm\pi/2$.

SNR_4 for QPSK signals ($p = 1$) with arbitrary η over the whole range of SNR can be derived from (5), (A9), and (A10) in Appendix A. To simplify the QPSK result for low SNR the terms in SNR^3 and SNR^4 in the denominator of (5) are dropped, giving

$$SNR_4 = \frac{(R/32B)[3\beta_{22} - \beta_4]^2 F^4 \, SNR^4}{2\eta^3 + 8\eta^2 F \, SNR + 3[\beta_4 + \beta_{22}]\eta F^2 \, SNR^2}. \quad (7)$$

For the most useful range of applications ($\eta \geq 1$ and SNR ≤ 0 dB), the maximum error in SNR_4 using this approximation is 0.3 dB (which occurs at $\eta = 1$ and SNR = 0 dB).

III. Experimental Confirmation

A. Methods

A carrier frequency $f = 70$ MHz was chosen to make use of available equipment. A detection bandwidth of $B = 10$ Hz was also used (but at high SNR, results with $B = 1$ kHz were scaled to $B = 10$ Hz, as explained in [1]). The results in this paper and [1] were all obtained with a set of tubular LC band-pass filters. Here we present results from one filter with the chip rate R set to give $\eta = 1$ (which was previously shown to be nearly optimum [1]), i.e., $W = R = 5.2$ MHz. ($R/B = 5.2 \times 10^5 = 57$ dB.) A description of the physical nonlinear device and the SNR measurement technique is found in [1].

The quadrature modulator, illustrated in [4, Fig. 3.] was composed of two separate arms, each with an attenuator after the corresponding BPSK modulator and before the two channels were combined. Attenuators with 0.1-dB steps were used to precisely adjust p to define the sharp nulls in $2f$ and $4f$ power. Experiments showed that the two paths from the split of carrier power at the input to the modulator to the summing of the two channels at the combiner must be well matched in electrical length. For example, the removal of 30 cm of cable (30° of carrier phase at 70 MHz) severely reduced the depth of the resonant null in $4f$ and changed p_{null}. The removal of only 3 cm of cable length (a 3° phase change) reduced the strength of the $2f$ null at $p = 1$ by 25 dB.

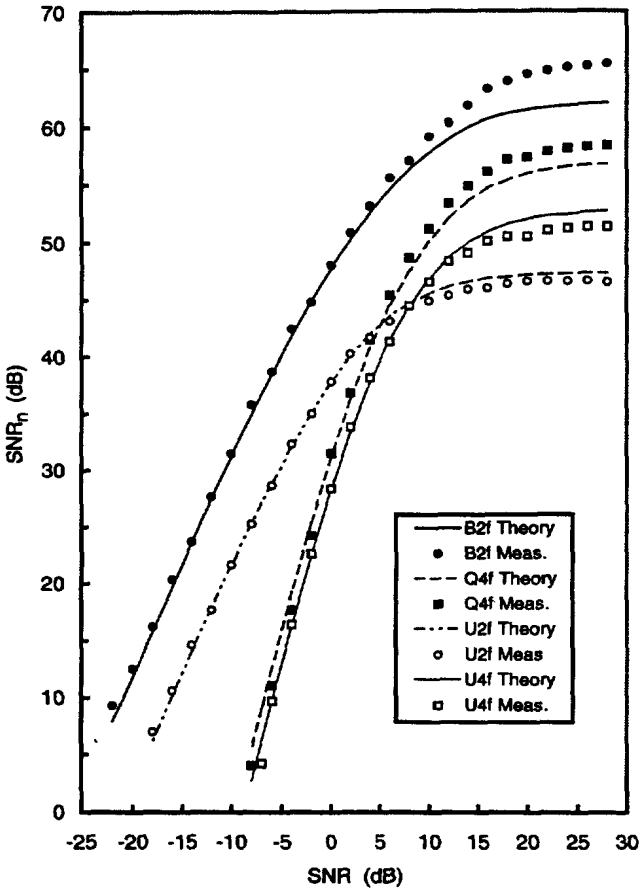

Fig. 2. SNR_n of detected carrier components ($n = 2$ or 4) vs input SNR. Detection of $2f$ for BPSK ($B2f$), $4f$ for QPSK ($Q4f$) and both components for UQPSK ($U2f$ and $U4f$) with $p = 0.5$ or -3 dB $\eta = 1$. $R/B = 57$ dB.

B. Results

A previous paper [1] showed that the use of a commercial modulator would aid an interceptor through modulator imperfections: local oscillator leak-through of the $1f$ component and creation of a detectable $2f$ component of imperfect QPSK signals through as little as 0.3 dB of channel power unbalance or 3° of phase unbalance. It also showed that for SNR ≤ 0 dB, the optimum value of η is about 1.0 ± 0.3. Since low SNR values are of greatest interest, $\eta = 1$ was used in most measurements and discussions in this report. The analytic theory applies to arbitrary η.

The detectability of a typical UQPSK signal ($p = -3$ dB) was measured at $2f$ and $4f$ as a function of SNR for $\eta = 1$. The results are presented in Fig. 2 where they may be compared with those for $2f$ detection of BPSK and $4f$ detection of QPSK. For SNR < 0 dB, theory and all measurements agree within 1 dB. The $4f$ component of UQPSK is only 2 dB less detectable than that of QPSK. The $2f$ component of UQPSK is 10 dB less detectable than that of BPSK. Using $SNR_n = 10$ dB as the threshold of detection, the order of detectability (from most detectable to least) of the four cases at low SNR is BPSK-$2f$, UQPSK-$2f$, QPSK-$4f$ and UQPSK-$4f$. The corresponding detection thresholds (for $R/B = 57$ dB) are SNR values of -24, -16, -7, and -6 dB, respectively. The slopes of the curves reach the theoretical 2.0 dB/dB for both $2f$ curves, but only reach 3.6 dB/dB for the $4f$ curves (compared to the very low

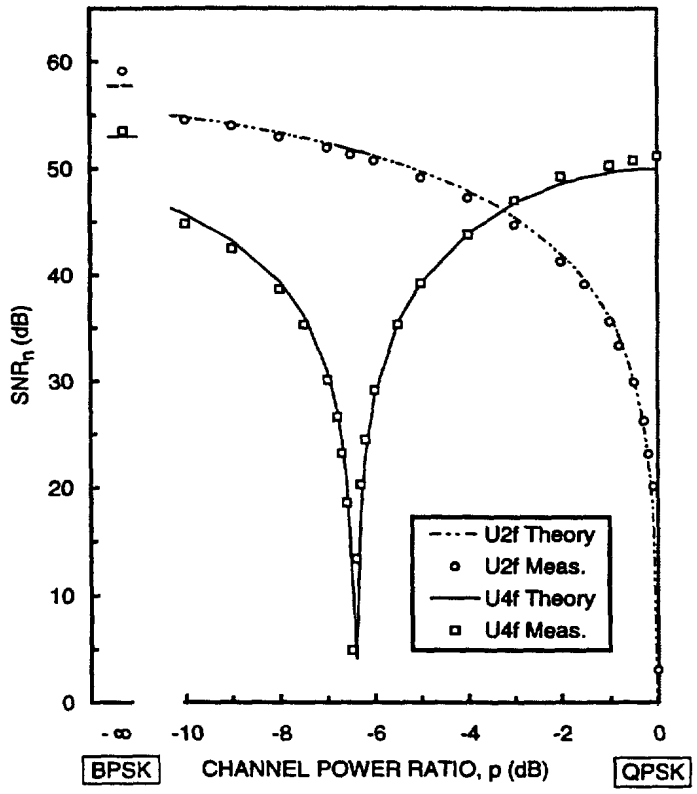

Fig. 3. SNR_n for the $n = 2$ and 4 carrier components of the UQPSK signal as a function of channel power ratio, p. $\eta = 1$. $R/B = 57$ dB. $\mathrm{SNR} = 10$ dB

SNR limit of 4.0 dB/dB). The highest reasonable interceptor's process gain of 80 dB gives a calculated slope of 3.9 dB/dB at $\mathrm{SNR}_4 = 10$ dB.

For SNR > 10 dB, the four curves asymptotically approach the self-noise limits. The limits for UQPSK are lower because the self-noise terms S_2 and S_4 (defined in Appendix A) are greater for $p > 0$. These limits are predicted less accurately by the theory, but still within 1.5 dB, except for the BPSK-$2f$ case, which is high by 3.5 dB. In that case, the limit could be reached by lowering β_4 to be 1.145 [in (3)] but this value would not fit the $4f$ null position of Fig. 3.

The effect of UQPSK channel power ratio on the detection of $2f$ power is shown in Fig. 3 for $\eta = 1$ and SNR $= 10$ dB. The predicted null in $2f$ is clearly visible. (A high SNR value was used to define the null very well.) The dominant factor is $(1-p)^2$ in the numerator of (2). The sharpness of the null shows how a typical channel unbalance of about 0.3 dB can dramatically increase the detectability of the $2f$ component of QPSK signals.

The effect of UQPSK channel power ratio on the detection of $4f$ power is also shown in Fig. 3. The sharp null in $4f$ power (with $\eta = 1$) is clearly seen at $p_{\mathrm{null}} = -6.5$ dB. The measured channel power ratios which extinguish the $4f$ power at other values of η are presented in Table I. The nulls have a depth >30 dB for all η. For virtually unfiltered signals ($\eta = 20$), $p_{\mathrm{null}} = -7.6 \pm 0.1$ dB, in excellent agreement with the theoretical prediction, -7.66 dB. The only discrepancy between theory and measurement is at $\eta = 0.50$, where p_{null} is -4.4 dB theoretically and -3.9 ± 0.1 dB experimentally. The measured p_{null} is -4.4 dB when $\eta = 0.60$.

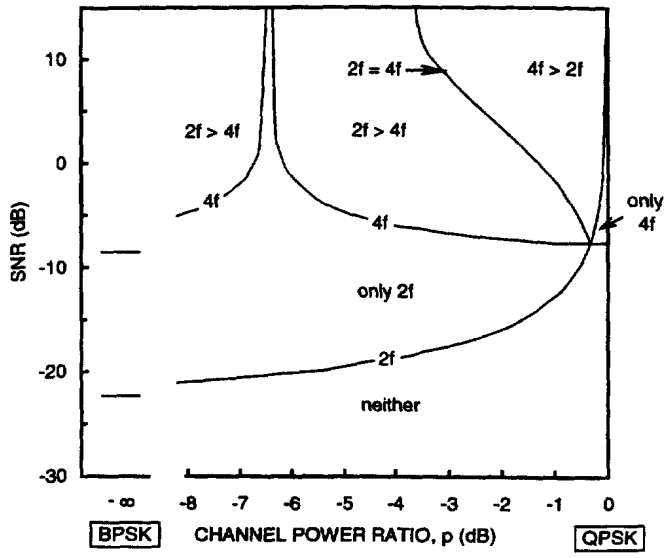

Fig. 4. Regions of carrier detectability for UQPSK signals as a function of SNR and channel power ratio. Detection threshold is $\mathrm{SNR}_n = 10$ dB. $\eta = 1$. $R/B = 60$ dB.

IV. Discussion and Conclusions

Theoretical detection performance boundaries, functions of both SNR and p, are presented in Fig. 4 for the case of $\eta = 1$ and $R/B = 60$ dB. They consist of the detection thresholds for the $2f$ and $4f$ components and the line defining equal detectability for those two components. The detection threshold for $2f$ approaches infinity at $p = 0$ dB, but lies below the detection threshold for $4f$ for all $p < -0.4$ dB. The detection threshold line for $4f$ approaches infinity at $p = -6.4$ dB, the location of the null in $4f$ power for $\eta = 1$. The third performance boundary, that of equal detectability of $2f$ and $4f$, is also marked. Note that it asymptotically approaches SNR $= \infty$ at $p = -3.7$ dB. For $p < -3.7$ dB, the signal is more detectable at $2f$ than at $4f$ for all SNR. The three lines define four regions of signal detectability: only $2f$ detectable, only $4f$ detectable, both detectable but $2f$ more detectable (denoted "$2f > 4f$"), and both detectable but $4f$ more detectable (denoted "$4f > 2f$"). One region of nondetectability (denoted "neither") is also defined, at low SNR for most values of p but at higher SNR near $p = 0$ dB. Balanced, or nearly balanced, QPSK signals are less detectable by nonlinear carrier detection techniques than any other type of UQPSK signal. While Fig. 4 applies to the specific case of $R/B = 60$ dB, $\eta = 1$, and detection SNR $= 10$ dB, similar performance diagrams drawn for other values of those parameters would not differ qualitatively from Fig. 4.

The minimum detectable SNR of BPSK and balanced QPSK signals detected by both carrier and chip-rate detectors over the complete practical range of interceptor's process gain (R/B) is illustrated in Fig. 5. Carrier detection boundaries are calculated from (4) and (7); the chip-rate detection boundary is calculated using a shift of 2 dB in input SNR for the same detected SNR, as shown in [3]. As the process gain (R/B) is varied from 40 to 80 dB, balanced QPSK is detectable at a threshold SNR ranging from -2 to -13 dB. Over the same range, BPSK is detectable at a threshold SNR varying from -12 to -32 dB.

In this paper, simple analytic expressions were derived for the detected SNR_2 or SNR_4 as a function of input SNR, channel

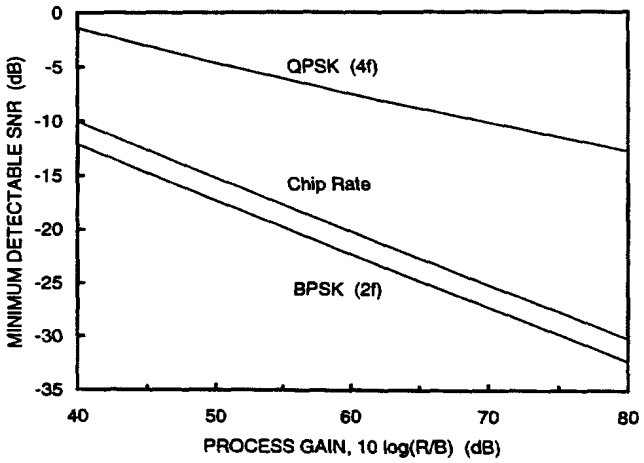

Fig. 5. Minimum detectable SNR of BPSK and QPSK signals as a function of interceptor's process gain, R/B. $\mathrm{SNR}_n = 10$ dB, $\eta = 1$.

power ratio p and normalized input bandwidth η. The theory assumed the transmitted signal was unfiltered, but this is a good approximation because the interceptor's optimum filtering, $\eta = 1$, is more narrow-band than the communicator's normal bandwidth filtering. The measurements presented here and in [1] and [4] confirm every aspect of the theory.

For unfiltered UQPSK, there is a sharp null in $4f$ power at the critical channel power ratio of $p_{\text{null}} = -7.66$ dB, the point at which the phase angle between the two channels is $\pi/8$. As band-pass filtering becomes more narrow (i.e., η decreases) p_{null} moves closer to unity, as illustrated in Table I. The $4f$ null cannot be used to hide the signal from carrier detection because at $p = p_{\text{null}}$, the $2f$ component is easily detected.

Regions of signal detectability were mapped as a function of SNR and p in Fig. 4. Balanced (or nearly balanced) ideal QPSK signals are less detectable by carrier detection techniques than either BPSK or UQPSK signals. Note, however, that the $1f$ component of nonideal QPSK signals may possibly be easily detected through modulator imperfections [1], and that the ideal QPSK signal is more strongly detected with the chip-rate detector (see Fig. 5).

Communicators using DSSS systems designed for low carrier detectability would need to use noncoherent despreading. The carrier of the despread signal, which has SNR > 0 dB, would be easily recoverable. To complete the design of a low-probability-of-detection DSSS communications system, additional work would be required on the reduction of chip-rate line detectability, perhaps by shaping or bandwidth limiting the baseband pulses [7], [8]. For low overall detectability in terms of both chip-rate and carrier components, the detectability of both should be studied together.

Appendix A
Theory of Carrier Detection for Unbalanced QPSK Signals

Within the detection system, at the point following the wide-band input band-pass filter, the input to the nonlinear device is defined as

$$\begin{aligned} x(t) &= s(t) + n(t) \\ s(t) &= s_a(t)\cos(2\pi ft) + s_b(t)\sin(2\pi ft) \\ n(t) &= n_a(t)\cos(2\pi ft) + n_b(t)\sin(2\pi ft) \end{aligned} \tag{A1}$$

where $s(t)$ is the signal, $n(t)$ is the noise, and f is the carrier frequency. In (A1), the baseband quadrature components of the signal are $s_a(t)$ and $s_b(t)$, and the baseband quadrature components of the noise are $n_a(t)$ and $n_b(t)$. Equation (A1) is the same as (1) when the substitutions $s_a(t) = \sqrt{P_a}c_a(t)d_a(t)$ and $s_b(t) = \sqrt{p}\sqrt{P_a}c_b(t)d_b(t)$ are made. For simplicity in the following calculations, $x(t)$ is rewritten as

$$\begin{aligned} x(t) &= a(t)\cos(2\pi ft) + b(t)\sin(2\pi ft) \\ a(t) &= s_a(t) + n_a(t) \\ b(t) &= s_b(t) + n_b(t) \end{aligned} \tag{A2}$$

where $a(t)$ and $b(t)$ are the quadrature components of the combined signal plus noise. For brevity, the explicit time dependence is normally suppressed and time averages are denoted by overbars.

The power of the baseband modulating signals (in a 1-Ω system) is given by $P_a = \overline{s_a^2}$; $P_b = \overline{s_b^2}$. The channel power ratio is defined as $p = P_b/P_a$. In the most general UQPSK case, $0 \le p \le 1$. The limiting cases are $p = 1$ for QPSK and $p = 0$ for BPSK. The radio frequency (RF) signal power P_s can be shown to be half of the total power of the modulating signal: $P_s = P_a(1 + p)/2$. The (chip energy)-to-(noise density) ratio at the input to the nonlinearity is $e \equiv P_s/N_0R$ where N_0 is the one-sided noise PSD and R the chip rate. SNR, the (chip energy)-to-(noise density) ratio at the input to the wide-band filter, is related to e by $e = F(\eta)\,\mathrm{SNR}$ where η is the ratio of input filter bandwidth to chip rate and $F(\eta)$ is the fraction of the signal power passing through an ideal filter of noise-equivalent bandwidth ηR and negligible passband loss. The rectangular transmitted pulses produce a sinc^2 power spectrum. Combining this with a brick-wall filter gives

$$F(\eta) = \int_{-\eta/2}^{\eta/2} \left(\frac{\sin(\pi x)}{\pi x}\right)^2 dx. \tag{A3}$$

The power of the modulating random noise processes is $P_n = \overline{n_a^2} = \overline{n_b^2} = \eta R N_0$, where the last equality results from the RF noise power being half the total power of the modulating noise components. The noise-to-signal power ratio, which is also useful, is $q \equiv P_n/P_a = \eta(1 + p)/(2e)$. The modulating noise processes, n_a and n_b, are independent identically-distributed zero-mean Gaussian random processes (with variance P_n), which gives

$$\begin{aligned} \overline{n_a} &= \overline{n_b} = 0 & \overline{n_a n_b} &= \overline{n_a}\,\overline{n_b} = 0 \\ \overline{n_a^2 n_b^2} &= \overline{n_a^2}\,\overline{n_b^2} = P_n^2 & \overline{n_a^4} &= \overline{n_b^4} = 3P_n^2 \\ \overline{n_a^6} &= \overline{n_b^6} = 15P_n^3 & \overline{n_a^8} &= \overline{n_b^8} = 105P_n^4 \end{aligned} \tag{A4}$$

where the coefficients 3, 15, and 105 apply to all zero-mean Gaussian distributions.

With no band-pass filtering, the baseband signals s_a and s_b, modeled as random processes, are independent streams of rectangularly shaped chips of equiprobable amplitudes $\pm\sqrt{P_a}$ or $\pm\sqrt{(pP_a)}$. Band-pass filtering, however, causes chip waveform distortion and intersymbol interference. Because of the timing dependence between s_a and s_b in the region of chip transitions, lower values of s_a^2 occur concurrently with lower values

of s_b^2, giving $\overline{s_a^2 s_b^2} \neq \overline{s_a^2}\,\overline{s_b^2}$. The signals are no longer statistically independent, but are still zero-mean ($\overline{s_a} = \overline{s_b} = 0$) uncorrelated ($\overline{s_a s_b} = 0$) and independent of the noise: $\overline{s_a^j n_a^k} = \overline{s_a^j}\,\overline{n_a^k}$; $\overline{s_b^j n_a^k} = \overline{s_b^j}\,\overline{n_a^k}$, etc., for all i and j. Because of equiprobable values in the unfiltered stream, all the odd powers of signals and odd moments of signal products average to zero. That is, $\overline{s_a^j} = \overline{s_b^j} = 0$ and $\overline{s_a^j s_b^k} = 0$ whenever j or k (or both) is odd. When j and k are both even, however, $\overline{s_a^j s_b^k} \neq 0$. Taking all of this into account, we defined two sets of normalized signal distortion coefficients

$$\beta_{jk} = \overline{s_a^j s_b^k} \Big/ \left(\overline{s_a^2}\right)^{\frac{j}{2}} \left(\overline{s_b^2}\right)^{\frac{k}{2}}, \qquad j,k \text{ even}$$

$$\beta_j = \overline{s_a^j} \Big/ \left(\overline{s_a^2}\right)^{\frac{j}{2}}, \qquad j = 4,6,8. \tag{A5}$$

The dependence of β_j and β_{jk} on η is implicit. Since the filtering affects s_a and s_b identically, $\beta_{jk} = \beta_{kj}$.

The two most important signal distortion coefficients are

$$\beta_4 \equiv \overline{s_a^4} \Big/ \left(\overline{s_a^2}\right)^2 = \overline{s_b^4} \Big/ \left(\overline{s_b^2}\right)^2$$

$$\beta_{22} = \overline{s_a^2 s_b^2} \Big/ \left(\overline{s_a^2}\,\overline{s_b^2}\right) \tag{A6}$$

since they control the position of the null in $4f$ (described below) and are the only distortion coefficients appearing in the calculated SNR_2 and SNR_4 for SNR < 0 dB. The general method of calculating the signal distortion coefficients is presented in Appendix B, and representative values of β_4 and β_{22} are presented in Table I.

For the second-order nonlinearity $(s+n)^2$ neglecting the baseband term is $y_2(t) = (1/2)(a^2 - b^2)\cos(4\pi ft) + ab\sin(4\pi ft)$. P_2, the total power of all components in the zone around $2f$, is equal to half the total power of the modulating signals

$$\begin{aligned} P_2 &= [\overline{((a^2-b^2)/2)^2} + \overline{(ab)^2}]/2 \\ &= \left(P_a^2/8\right)[(1+p^2)\beta_4 + 2p\beta_{22} + 8q(1+p+q)] \end{aligned}$$

P_2', the power of the discrete component at $2f$, is equal to half the total power of the dc component of the modulating signal: $P_2' = [(\overline{(a^2-b^2)/2})^2 + (\overline{ab})^2]/2 = (P_a^2/8)(1-p)^2$. The power of the continuous spectrum around $2f$, P_2'' is found by subtraction to be

$$P_2'' \equiv P_2 - P_2' = \left(P_a^2/8\right)[S_2 + 8q(1+p+q)]$$

where $S_2 \equiv [(1+p^2)(\beta_4 - 1) + 2p(\beta_{22}+1)]$, being independent of noise-to-signal ratio q is the self-noise component of the total noise power density at $2f$ (hence the designation S_2).

The input and processed spectra are presented in Fig. 6. With ideal rectangular band-pass filters, the noise spectrum is always rectangular. For simplicity in the calculation of PSD at the detection frequencies, the signal spectrum is also modeled as rectangular with bandwidth ηR and spectral density set for correct total RF power $F(\eta)P_s$. The generally good agreement of measurements with theory, even for large η, indicates that the error in this approximation is small.

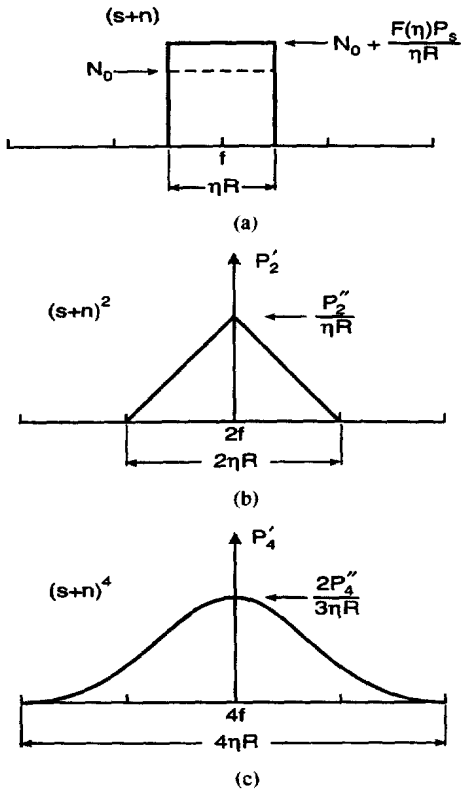

Fig. 6 Spectral components of signal (s) and noise (n) (a) simplified input spectrum of $(s+n)$; (b) components of $(s+n)^2$ near $2f$; and (c) components of $(s+n)^4$ near $4f$

With both the input signal and noise spectra rectangular with width ηR, the continuous spectrum at $2f$ (the convolution of the rectangle with itself) is triangular with base $2\eta R$. The area of the triangle is P_2'', and hence its height, which is the PSD at $2f$, is $\mathrm{PSD}_2 = P_2''/\eta R$. For detection bandwidth $B \ll \eta R$, the spectral density at $2f$ may be taken as constant across the detection bandwidth. This gives

$$\begin{aligned} \mathrm{SNR}_2 &= P_2'/[B \cdot \mathrm{PSD}_2] = (P_2'\eta R)/(P_2'' B) \\ &= \frac{(\eta R/B)(1-p)^2 e^2}{2\eta^2(1+p)^2 + 4\eta(1+p)^2 e + S_2 e^2} \\ &= \frac{(\eta R/B)e^2}{2\eta^2 + 4\eta e + [\beta_4 - 1]e^2}, \qquad \text{for } p = 0; \text{BPSK}. \end{aligned} \tag{A7}$$

For the fourth-order nonlinearity $(s+n)^4$ (neglecting terms near dc and $2f$) is $y_4(t) = (1/8)(a^4 - 6a^2b^2 + b^4)\cos(8\pi ft) + (1/2)ab(a^2 - b^2)\sin(8\pi ft)$. P_4, the total power of all components in the zone around $4f$, is equal to half the total power of the modulating signals, and reduces to

$$\begin{aligned} P_4 &= \frac{P_a^4}{128}[Q_0 + 32qQ_1 + 288q^2Q_2 \\ &\quad + 768q^3(1+p) + 384q^4] \end{aligned} \tag{A8}$$

$$Q_0 = (1+p^4)\beta_8 + 4p(1+p^2)\beta_{62} + 6p^2\beta_{44}$$

$$Q_1 = (1+p^3)\beta_6 + 3p(1+p)\beta_{42}$$

$$Q_2 = (1+p^2)\beta_4 + 2p\beta_{22} \tag{A9}$$

P_4', the power of the discrete component at $4f$, is equal to half the total power of the dc components of the modulating signals: $P_4' = (P_a^4/128)\gamma_4$ where

$$\gamma_4 = [\beta_4(1+p^2) - 6p\beta_{22}]^2. \tag{A10}$$

The power of the continuous spectrum around $4f$, P_4'' is found by subtraction to be

$$P_4'' \equiv P_4 - P_4' = (P_a^4/128)\,[S_4 + 32qQ_1 + 288q^2Q_2 + 768q^3(1+p) + 384q^4]$$

where $S_4 \equiv Q_0 - \gamma_4$ is the term in P_4'' which is independent of noise-to-signal ratio q and is therefore the self-noise component of the PSD near $4f$. The continuous spectrum near $4f$ is twice the autoconvolution of the triangular PSD near $2f$. It can be derived as a series of quadratic terms by piecewise integration, but the shape, illustrated in Fig. 6(c), was easier to derive using MATLAB or a spreadsheet. We are interested only in the density at $4f$, which is twice the integral of the square of the triangular density at $2f$, or $\mathrm{PSD}_4 = 2P_4''/(3\eta R)$. The predicted SNR_4 is therefore (A11), shown at the bottom of the page. At high e, $\mathrm{SNR}_4 \to$ constant, and at low e, $\mathrm{SNR}_4 \propto e^4$. When band-pass filtering is weak, $\eta \gg 1$ and all β_{jk} and $\beta_j \to 1$, giving $S_4 \to 16p(1-p)^2$. The self noise S_4 is therefore zero (for $\eta \gg 1$) for both limiting cases of interest: $p = 0$ (BPSK) and $p = 1$ (QPSK). S_4 is >0 for all other p (and $\eta \gg 1$). This explains the lower values of the asymptotic SNR_2 and SNR_4 at high SNR in Fig. 2.

Appendix B
Evaluation of Signal Distortion Coefficients

The signal distortion coefficients defined in (A5) and (A6) are easy to evaluate for the two extreme limits, $\eta = \infty$ and 0. At the unfiltered limit ($\eta = \infty$), the rectangular pulses are undistorted so that all $\beta_j = 1$. The independent random binary sequences give all $\beta_{ij} = \beta_i\beta_j$, which gives $\beta_{ij} = 1$ from the previous result. At the opposite extreme, as $\eta \to 0$, the filtered signal contains contributions from a very large number of independent transmitted pulses. Thus, from the central limit theorem, the baseband waveforms approach independent zero-mean Gaussian random processes. From the zero-mean Gaussian properties and (A4), $\beta_4 = 3$. From the independence property, $\beta_{22} = 1$.

A. Outline of Calculation

For all cases between the two limits, we must develop the general theory and then evaluate the formulas for specific models. The end-to-end system response is modeled in three stages. First, a series of data impulses are fed into the transmitter low-pass filter, which has impulse response $T(t)$. That is, the baseband version of the transmitted data pulse is $T(t)$. Secondly, we assume that the upconversion, RF transmission over the physical channel, and downconversion in the receiver cause no distortion in the pulse shape. We also ignore the channel propagation delays and power loss, which have no effect on the calculation. Finally, the effect of the carrier detection system's receiver band-pass filter is modeled as the effect of the corresponding low-pass filter, which has impulse response $R(t)$. The composite effect of the whole channel, from the transmitter's baseband input impulse at time $t = 0$ to the receiver's baseband-equivalent output, is represented by the composite impulse response function

$$h(t) = \int_{-\infty}^{\infty} T(\tau)R(t-\tau)\,d\tau. \tag{B1}$$

We assume that the transmitted impulses occur at times $t = i$, where i ranges over all integer values. The baseband components of the RF signals at the input to the receiver's nonlinearity are

$$s_a(t) = \sum_i a_i h(t-i) \qquad s_b(t) = \sum_i b_i h(t-i) \tag{B2}$$

where

$$a_i = \pm 1 \qquad b_i = \pm\sqrt{p} \tag{B3}$$

are the amplitudes of the quadrature impulses transmitted at time i. A comparison with the text following (A1) shows that the A-channel amplitude $\sqrt{P_a}$ has been neglected since the absolute amplitude has no effect on the signal distortion coefficients.

We calculate the joint moments of the baseband signals $s_a(t)$ and $s_b(t)$

$$\alpha_{mn} \equiv \overline{\langle s_a^m(t)s_b^n(t)\rangle} \tag{B4}$$

(for integers m and n, both even and ≥ 2) where $\langle\cdot\rangle$ indicates statistical expectation over the ensemble of all possible sequences of data bits. Note that when the time dependence (t) is explicitly included within the expectation operator, it indicates that the value is the expectation at time t, not the overall time-averaged expectation, which is denoted by the overbar. The normalized moments, or signal distortion coefficients, can then be calculated from (B4) and (A5) as

$$\beta_{mn} \equiv \alpha_{mn} \Big/ \left(\alpha_{20}^{m/2} \cdot \alpha_{02}^{n/2}\right). \tag{B5}$$

We also assume that a_i and b_j are statistically independent over the ensemble of all possible sequences of bits for all i and j, and hence $\langle a_i b_j\rangle = 0$. Since a_i and a_j (and similarly b_i and b_j) are independent for $i \neq j$, then from (B3)

$$\langle a_i a_j\rangle = \delta_{ij} \qquad \langle b_i b_j\rangle = p\delta_{ij}$$
(where $\delta_{ij} = 1$ when $i = j$ and 0 otherwise). (B6)

$$\mathrm{SNR}_4 = P_4'/[\beta \cdot \mathrm{PSD}_4] = (3\eta R P_4')/(2BP_4'') = \frac{(3\eta R/2B)\gamma_4 e^4}{24(1+p)^4\eta^4 + 96(1+p)^4\eta^3 e + 72(1+p)^2Q_2\eta^2e^2 + 16(1+p)Q_1\eta e^3 + S_4e^4} \tag{A11}$$

Since the transmitted impulses occur at uniform intervals and are independent, the statistics are the same at a given position within each interval. That is, $\langle s_a^m(t)s_b^n(t)\rangle = \langle s_a^m(t-i)s_b^n(t-i)\rangle$ for all integers i. The expectation averaged over all time is therefore equal to the average over any one symbol duration. For simplicity here, the symbol duration is normalized to one unit, so that time averages are over the interval $[0,1]$.

B. Calculation of Signal Moments

We now calculate in turn the four most useful joint moments: $\alpha_{20}, \alpha_{02}, \alpha_{22}$, and α_4 ($\equiv\alpha_{40}$), and from them, β_{22} and β_4.

First, we evaluate α_{20} using (B2) and (B4)

$$\begin{aligned} s_a^2(t) &= \left[\sum_i a_i h(t-i)\right]\cdot\left[\sum_j a_j h(t-j)\right] \\ &= \sum_i\sum_j a_i a_j h(t-i)h(t-j) \\ \langle s_a^2(t)\rangle &= \sum_i\sum_j \langle a_i a_j\rangle h(t-i)h(t-j) \\ &= \sum_i h^2(t-i), \qquad \text{since } \langle a_i a_j\rangle = \delta_{ij} \text{ from (B6)} \end{aligned}$$

The time-averaged expectation is then

$$\alpha_{20} = \overline{\langle s_a^2(t)\rangle} = \int_0^1 \sum_i h^2(t-i)\,dt = \sum_i \int_0^1 h^2(t-i)\,dt.$$

Since the ranges of integration of the terms of the summation are contiguous, this is simply

$$\alpha_{20} = \int_{-\infty}^{\infty} h^2(\tau)\,d\tau \tag{B7}$$

which is the energy in the impulse response. From (B4) and (B6), we can easily show that

$$\alpha_{02} = p\alpha_{20}. \tag{B8}$$

Next, we evaluate α_{22}

$$\begin{aligned} s_a^2(t)s_b^2(t) &= \left[\sum_i a_i h(t-i)\right]\cdot\left[\sum_j a_j h(t-j)\right] \\ &\quad\cdot\left[\sum_k b_k h(t-k)\right]\cdot\left[\sum_l b_l h(t-l)\right] \\ &= \sum_i\sum_j\sum_k\sum_l a_i a_j b_k b_l \\ &\quad\times h(t-i)h(t-j)h(t-k)h(t-l) \\ \langle s_a^2(t)s_b^2(t)\rangle &= \sum_i\sum_j\sum_k\sum_l \langle a_i a_j\rangle\langle b_k b_l\rangle \\ &\quad\times h(t-i)h(t-j)h(t-k)h(t-l) \\ &= p\sum_i\sum_k h^2(t-i)h^2(t-k) \qquad \text{using (B6)} \\ \alpha_{22} &= \overline{\langle s_a^2(t)s_b^2(t)\rangle} \\ &= p\int_0^1 \sum_i\sum_k h^2(t-i)h^2(t-k)\,dt \\ &= p\sum_i\sum_k \int_0^1 h^2(t-i)h^2(t-k)\,dt. \end{aligned}$$

Substituting $w = k-i$, and then $\tau = t-i$, and utilizing contiguous intervals gives

$$\alpha_{22} = p\sum_w \int_{-\infty}^{\infty} h^2(\tau)h^2(\tau-w)\,d\tau. \tag{B9}$$

For convenience, we normalize α_{22} to remove the dependence on p

$$\hat{\alpha}_{22} = \alpha_{22}/p = \sum_w \int_{-\infty}^{\infty} h^2(\tau)h^2(\tau-w)\,d\tau. \tag{B10}$$

In the expression for $\hat{\alpha}_{22}$, the sum is over all integer (bit time) lags. In particular, the terms with $w \neq 0$ contain the effects of intersymbol interference. From (B5), the value of β_{22} is then

$$\beta_{22} \equiv \alpha_{22}/(\alpha_{20}\cdot\alpha_{02}) = \hat{\alpha}_{22}/\alpha_{20}^2 \tag{B11}$$

since the factors of p in the numerator and denominator cancel when substitutions are made using (B10) and (B8). β_{22} is independent of p.

Finally, we evaluate $\alpha_4 \equiv \alpha_{40}$

$$\begin{aligned} s_a^4(t) &= \left[\sum_i a_i h(t-i)\right]\cdot\left[\sum_j a_j h(t-j)\right] \\ &\quad\cdot\left[\sum_k a_k h(t-k)\right]\cdot\left[\sum_l a_l h(t-l)\right] \\ &= \sum_i\sum_j\sum_k\sum_l a_i a_j a_k a_l \\ &\quad\times h(t-i)h(t-j)h(t-k)h(t-l) \\ \langle s_a^4(t)\rangle &= \sum_i\sum_j\sum_k\sum_l \langle a_i a_j a_k a_l\rangle \\ &\quad\times h(t-i)h(t-j)h(t-k)h(t-l). \end{aligned}$$

This is similar to the corresponding expression for α_{22}. However, there are now more combinations of $\{i,j,k,l\}$ for which the expectation $\langle a_i a_j a_k a_l\rangle$ is nonzero. Specifically, the mutually exclusive combinations are $\{i=j, k=l$ for all i and $k\}$, $\{i=k, j=l, i\neq j\}$, and $\{i=l, j=k, i\neq j\}$, giving

$$\begin{aligned} \langle s_a^4(t)\rangle &= \sum_i\sum_k h^2(t-i)h^2(t-k) \\ &\quad+\sum_i\sum_j h^2(t-i)h^2(t-j) - \sum_i h^4(t-i) \\ &\quad+\sum_i\sum_j h^2(t-i)h^2(t-j) - \sum_i h^4(t-i) \\ &= 3\sum_i\sum_j h^2(t-i)h^2(t-j) - 2\sum_i h^4(t-i) \\ \alpha_4 &= \overline{\langle s_a^4(t)\rangle} = 3\sum_i\sum_j \int_0^1 h^2(t-i)h^2(t-j)\,dt \\ &\quad - 2\sum_i \int_0^1 h^4(t-i)\,dt. \end{aligned}$$

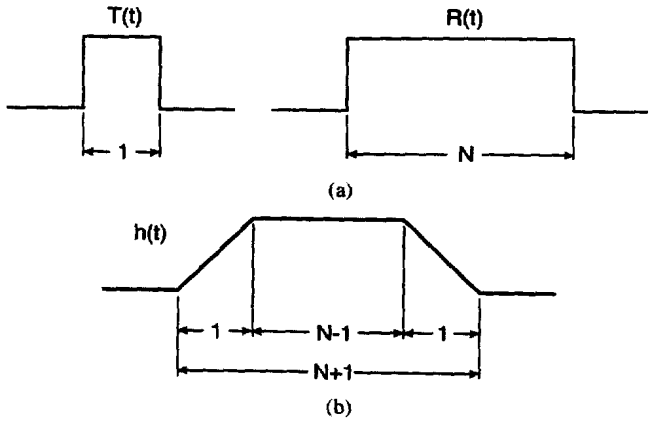

Fig 7. Rectangular impulse response model Low-pass impulse response functions of: (a) transmitter $T(t)$ and receiver $R(t)$ and (b) composite channel [convolution of $T(t)$ with $R(t)$].

TABLE II
SIGNAL DISTORTION COEFFICIENTS β_{22} AND β_4 FOR RECTANGULAR- AND BUTTERWORTH-RESPONSE FILTERS ($N = \eta^{-1}$)

η	N	β_{22}		β_4	
		Rectangular	Butterworth	Rectangular	Butterworth
0	∞	1	1	3	3
1/3	3	1.003	—	2.334	—
1/2	2	1.008	1.00	2.016	1.93
1	1	1.050	1.018	1.350	1.325

From (B10) and the text preceeding it

$$\alpha_4 = 3\hat{\alpha}_{22} - 2\int_{-\infty}^{\infty} h^4(\tau)\,d\tau. \tag{B12}$$

Finally

$$\beta_4 = \alpha_4 / \alpha_{20}^2 . \tag{B13}$$

The variables $\hat{\alpha}_{22}, \alpha_{20}, \alpha_4$, and β_4 are all independent of p. If β_4 were calculated for the B channel instead of the A channel, it would be $\alpha_{04}/\alpha_{02}^2$, and a factor of p^2 in both numerator and denominator would cancel, again giving (B13) for the answer.

It may be seen in (B10) for $\hat{\alpha}_{22}$, that a sum must be made over all lags, which can extend from 3 to 10 bit durations in realistic cases. The calculations for higher-order coefficients α_{mn} and β_{mn} are even more complex. Thus, in most realistic cases, the expressions are too difficult to evaluate analytically. In most cases they must be evaluated by simulation or numerical evaluation. For the higher-order coefficients in particular, simulation is easier.

C. Applications

A simple case that can be evaluated analytically is illustrated in Fig. 7. Since transmitter band-pass filtering is assumed to be very weak, $T(t)$ is assumed to be rectangular. For convenience, we assume these pulses have unit width and the receiver impulse response $R(t)$ is a rectangular pulse of length N bit durations. $\eta = 1/N$. The special case of $N = \eta = 1$ corresponds to matched filtering. For this model, $h(t)$ calculated from (B1) is trapezoidal and the alphas are calculated from (B7), (B10), and (B12) to be

$$\begin{aligned} \alpha_{20} &= N - 1/3 \\ \hat{\alpha}_{22} &= N^2 - 2N/3 + 2/15 \\ \alpha_4 &= 3N^2 - 4N + 8/5 \end{aligned} \tag{B14}$$

so that the betas, calculated from (B11) and (B13), are

$$\begin{aligned} \beta_{22} = \hat{\alpha}_{22}/\alpha_{20}^2 &= (N^2 - 2N/3 + 2/15)/(N - 1/3)^2 \\ \beta_4 = \alpha_4/\alpha_{20}^2 &= (3N^2 - 4N + 8/5)/(N - 1/3)^2. \end{aligned} \tag{B15}$$

The evaluation of these coefficients for different values of N is presented in Table II, where the corresponding values for the third-order Butterworth filter (from Table I) are also presented. The coefficients for the rectangular and Butterworth pulse shapes are remarkably similar. For the rectangular receiver pulse shape, β_{22} is always close to 1.00, and approaches 1 as $\eta \to 0$. At the same limit, $\beta_4 \to 3$, the theoretical limit for Gaussian distributions.

Our five-stage tubular LC band-pass filters were modeled as third-order Butterworth filters and all the coefficients were calculated using standard simulation techniques. The variation of β_4 and β_{22} with η is presented in Table I. For the most important case of $\eta = 1$, $F(1) = 0.773$, and the distortion coefficients for our model are $\beta_{22} = 1.018, \beta_4 = 1.325, \beta_{42} = 1.332, \beta_{44} = 1.760, \beta_{62} = 1.886, \beta_6 = 1.903$, and $\beta_8 = 2.854$.

ACKNOWLEDGMENT

REFERENCES

[1] D. A. Hill and J. B. Bodie, "Experimental carrier detection of BPSK and QPSK direct sequence spread spectrum signals," in *Conf Rec. MILCOM'95*, vol. 1, Nov. 1995, pp. 362–367.
[2] W. A. Gardner and C. M. Spooner, "Signal interception: Performance advantages of cyclic-feature detectors," *IEEE Trans Commun.*, vol. 40, pp. 149–159, Jan. 1992.
[3] D. A. Hill and E. B. Felstead, "Laboratory performance of spread spectrum detectors," *Proc. Inst. Elect. Eng.—Commun.*, vol. 142, pp. 243–249, Aug. 1995.
[4] D. A. Hill and J. B. Bodie, "Carrier detection of unbalanced QPSK direct sequence signals," in *Conf. Rec. MILCOM'99*, 1999.
[5] A. P. Clark, "Carrier-phase synchronization in the demodulation of UQPSK signals," *Proc Inst. Elect Eng.*, pt. I, vol. 136, pp. 351–360, Oct. 1989.
[6] J. F. Oberst and D. L. Schilling, "The SNR of a frequency doubler," *IEEE Trans. Commun. Technol.*, vol. COM-19, pp. 97–99, Feb. 1971.
[7] J.-C. Imbeaux, "Performances of the delay-line multiplier circuit for clock and carrier synchronization in digital satellite communications," *IEEE J. Select. Areas Commun.*, vol. SAC-1, pp 82–95, Jan. 1983
[8] D. E. Reed and M. A Wickert, "Spread spectrum signals with low probability of chip rate detection," *IEEE J Select. Areas Commun.*, vol. 7, pp 595–601, May 1989

Douglas A. Hill received the B Sc. degree in mathematics and physics from the University of Toronto, Toronto, ON, Canada, in 1966, and the Ph.D. degree in physics from the University of British Columbia, Vancouver, BC, Canada, in 1972.

Most of his career has been with Defence Research and Development Canada, at the Defence Research Establishment Ottawa, Ottawa, ON, Canada He often contributes papers to the IEEE Conferences on Military Communications His research interests include the detection and jamming of frequency-hopping and direct-sequence spread-spectrum communications signals.

Dr. Hill is currently an affiliate of the IEEE Communications Society and a member of the Armed Forces Communications Electronics Association.

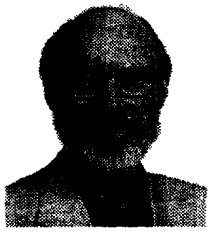

John B. Bodie was born in Winnipeg, MB, Canada, in 1950. He received the B.Sc. degree in electrical engineering from the University of Manitoba, Winnipeg, MB, Canada, in 1972, and the M.Eng. degree from McMaster University, Hamilton, ON, Canada, in 1974

His work has been primarily in the development of instrumentation for satellite and radio communications systems In 1995, he co-founded Square Peg Communications Inc., Ottawa, ON, Canada, which specializes in equipment for the mobile satellite communications industry.

#516581

CA011982